

Concept-based model explanations for Electronic Health Records

Sebastien Baur^{*†}

Shaobo Hou^{*‡}

Eric Loreaux^{*†}

Diana Mincu^{*†}

Anne Mottram[†]

Ivan Protsyuk[†]

Nenad Tomasev[†]

Martin G Seneviratne[†]

Alan Karthikesanlingam[†]

Jessica Schrouff^{†§}

SEBASTIENBAUR@GOOGLE.COM

SHAOBOHOU@GOOGLE.COM

ELOREAU@GOOGLE.COM

DMINCU@GOOGLE.COM

ANNEMOTTRAM@GOOGLE.COM

IPROTSYUK@GOOGLE.COM

NENADT@GOOGLE.COM

MARTSEN@GOOGLE.COM

ALANKARTHI@GOOGLE.COM

SCHROUFF@GOOGLE.COM

Abstract

Recurrent Neural Networks (RNNs) are often used for sequential modeling of adverse outcomes in electronic health records (EHRs) due to their ability to encode past clinical states. These deep, recurrent architectures have displayed increased performance compared to other modeling approaches in a number of tasks, fueling the interest in deploying deep models in clinical settings. One of the key elements in ensuring safe model deployment and building user trust is model explainability. Testing with Concept Activation Vectors (TCAV) has recently been introduced as a way of providing human-understandable explanations by comparing high-level concepts to the network’s gradients. While the technique has shown promising results in real-world imaging applications, it has not been applied to structured temporal inputs. To enable an application of TCAV to sequential predictions in the EHR, we

propose an extension of the method to time series data. We evaluate the proposed approach on an open EHR benchmark from the intensive care unit, as well as synthetic data where we are able to better isolate individual effects.

Keywords: Explainability, neural networks, human concepts, electronic health records (EHR)

1. Introduction

Wider availability of Electronic Health Records (EHR) has led to an increase in machine learning applications for clinical diagnosis and prognosis (e.g., [Ambrosino et al., 1995](#); [Caruana et al., 2015](#)). Larger de-identified datasets and public benchmarks have fueled the application of increasingly complex techniques such as recurrent neural networks (RNNs) to predict adverse clinical events (e.g., [Lipton et al., 2016](#); [Xiao et al., 2018](#); [Shickel et al., 2019](#); [Futoma et al., 2017](#); [Tomašev et al., 2019](#)). RNNs can operate over a sequence of health information, iteratively combining input data with internal memory states to generate new states, mak-

* Equal contribution, by alphabetical order.

† Google Health

‡ DeepMind

§ Google Research, Brain team

ing them suitable for continuous clinical predictions. While these memory-storing networks allow for accurate and dynamic predictions, it is often difficult to examine the mechanism by which clinical information is being translated into outputs. In healthcare, as in other fields in which trust is paramount, it is not sufficient to show state of the art discriminative performance; clinicians have also deemed it critical that models provide local and global *explanations* for their behavior (Tonekaboni et al., 2019).

Multiple approaches have been proposed to provide explanations for machine learning models applied to EHR data (see Payrovnaziri et al., 2020, for a review), with a focus on attention-based methods when the architecture relies on RNNs (e.g., Choi et al., 2016; Sha and Wang, 2017; Shickel et al., 2019). Typically, those interpretability techniques ranks the input features based on their attention scores. However, single feature rankings might not highlight clinical states that encompass multiple input features (e.g. “infection”) in an intuitive manner. To address this issue of human understandability, Panigutti et al. (2020) use an ontology of diagnoses to provide insights across single features. This approach, however, relies on diagnoses which are typically recorded at the end of an admission and is therefore not suitable to identify temporal changes across features that reflect a clinical concept, nor is it able to provide continuous predictions.

On the other hand, human-understandable explanations have been successfully developed for computer vision applications: Testing with Concept Activation Vectors (TCAV, Kim et al., 2018) relies on human-understandable “concepts” to derive model explanations. Practitioners or end users can select examples from the data that embody intuitive concepts (e.g. “pointy ears” or “stripes”), and these examples are then used

to map concepts to the model’s activation space in the form of concept activation vectors (CAVs). CAVs can then be used to provide global explanations, as well as assess the presence or absence of a concept in local examples.

In this work, we define “clinical concepts” from temporal EHR input features to improve the human-understandability of post-hoc explanations of continuous clinical predictions. Our approach leverages TCAV (Kim et al., 2018) and can be applied to previously trained models without restrictions on model inputs or RNN architecture. Our contributions are as follows:

- We extend the TCAV approach to the time series setting.
- We design a synthetic time series dataset to evaluate (concept-based) attribution methods.
- We demonstrate that the proposed technique reflects the ground truth on synthetic data.
- We propose a framework to define human-understandable concepts in EHR and illustrate it using the de-identified MIMIC-III benchmark dataset (Johnson et al., 2016b).

2. Methods

Notation: We consider a set of multivariate time series $\mathcal{X} := (x_{i,t,d})_{i \leq N, t \leq T_i, d \leq D}$, where $x_{i,t,d} \in \mathbb{R}$, N is the number of time series (i.e. patients), D is the number of features per time step and T_i the number of time steps for patient i . We define \mathbf{x}_i as the time series for feature $d \in \{1, \dots, D\}$ for a single example. The label $\mathbf{y} \in \{0, 1\}^{N \times T}$ exists for all examples and all time steps. We train a recurrent neural network $F : \mathcal{X} \rightarrow [0, 1]^T$ with L layers. For a given layer $1 \leq l \leq L$ and time step $1 \leq t \leq T$, we can write the

predicted output of F as $F_t(\mathbf{x}) := h(f_l(\mathbf{x}_{1:t}))$ where $f_l(\mathbf{x}_{1:t})$ is the activation vector at the l -th layer after t time steps, further referred to as $\mathbf{a}_{t,l}$ and h represents the operations in layers $l \dots L$. Please note that we consider binary classification settings, but the approach extends to multi-class predictions.

2.1. Concept-based explanations over time

In this section, we extend TCAV (Kim et al., 2018) to account for the temporal dimension. TCAV relies on two main steps: (1) Building a concept activation vector (CAV) for each concept, and (2) assessing how the concept influences the model’s decision.

Building a CAV: To build a CAV, Kim et al. (2018) sample positive and negative examples for a concept, record their activations \mathbf{a}_l at each layer l and build a linear classifier distinguishing between activations related to positive and negative samples. To extend this approach to timeseries, we identify a ‘time window of interest’ $[t_{start}, t_{end}]$ that reflects a trajectory corresponding to a concept, i.e. during which some features or feature changes are present. We define a ‘control’ group as a set of trajectories in which the concept does not manifest. We then collect the model’s activations from $t = t_{start}$ to the end of the window t_{end} for both groups, and training data for CAV learning is defined based on three different strategies:

- $CAV_{t_{end}}$: we record the model’s activations in each layer at t_{end} . This reflects the assumption that the trajectory can be represented by its end point.
- $CAV_{t_{start}:t_{end}}$: we record the model’s activations at each time step between t_{start} and t_{end} , using them as samples in the linear classifier. This approach hypothesizes that each time step in the trajec-

tory represents a key component of the concept pattern.

- $CAV_{t_{end}-t_{start}}$: we record the model’s activations at t_{start} and at t_{end} and use their difference to train the CAV. In this case, we assume that changes in activations represent the concept of interest.

We assess the linear classifier’s performance using a bootstrap resampling scheme ($k=100$) and perform random permutations (1,000 permutations, 10 per bootstrap resampling) of the labels to obtain a null distribution of balanced accuracy and area under the receiver-operating curve (AUROC). We assess a CAV as significant if all metrics are higher than the estimated null distributions with $p < 0.05$. We then estimate the generalizability of the classifier across time steps by performing the classification at all time points ($t = 1, \dots, T$), where we give a label of 1 to all time points affected by a concept, and 0 for a control example.

Presence of the concept in a sample: The original TCAV work (Kim et al., 2018) computes the cosine similarity between the activations \mathbf{a}_l of a sample and the obtained CAV at each layer to estimate how similar an image is to a concept. If we assume a sample that can contain multiple concepts each represented by a CAV, this similarity measure can be thought of as estimating whether a concept is manifesting in the sample. In time series, it can be computed at each time point independently to obtain a (local) trajectory of concept presence per layer. We propose to estimate whether the activations move over time in the direction of the concept by computing the temporal Concept Angle (tCA):

$$tCA_C(\mathbf{x}_t, dt) = \frac{[\mathbf{a}_{l,t} - \mathbf{a}_{l,t-dt}]^T}{\|\mathbf{a}_{l,t} - \mathbf{a}_{l,t-dt}\|_2} \mathbf{v}_C$$

Where \mathbf{v}_C corresponds to the unit norm CAV of concept C and dt represents a con-

stant lag in a time shifting window. Please note that this difference can be smoothed.

Influence of the concept on the model’s prediction: Kim et al. (2018) define the Conceptual Sensitivity (CS), to estimate how the model’s gradients align with the CAV. This quantity, when aggregated over samples, represents a global explanation. Mathematically, CS can be computed as the directional derivative:

$$\begin{aligned} CS_{C,t}(F, \mathbf{x}_t) &:= \frac{\partial h(f_l(\mathbf{x}_t))}{\partial \mathbf{v}_C} \\ &= \nabla h(f_l(\mathbf{x}_t))^T \mathbf{v}_C \end{aligned}$$

Which amounts to computing the cosine similarity between the direction of the CAV and the model’s gradients. In the present case, CS is computed at every time step of the local trajectory by taking the gradients of the models w.r.t. the sigmoid of the logits. The obtained scores can be aggregated over time and/or over samples to obtain global concept attributions.

We believe that *tCA* and CS can be seen as providing complementary information for global explanations, i.e. how is the presence/absence of the concept varying across time, and is the model influenced by the presence/absence of the concept to make its decisions? Indeed, a concept being “present” does not guarantee that the model relies on it for prediction. On the other hand, a CS score of 0 means that affecting how present the concept is has (locally) no influence on the model output.

2.2. Synthetic timeseries

Inspired by (Goyal et al., 2019), we evaluate the proposed approach on a synthetic dataset designed to isolate individual effects.

Dataset design: In our setup, a concept C , akin to a latent variable, can manifest through a causal relationship with a

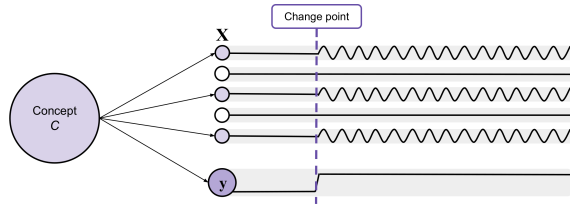


Figure 1: Illustration of the causal graph and sampling of time series for the synthetic dataset. A concept C affects a subset of features $i \in \{1, 3, 5\}$ and a label y after the ‘change point’.

time series’ features and label (see Figure 1). For simplicity, we consider a binary behavior for C : a concept either manifests and is “present” in a sample after a selected temporal “change point”, or it is “absent”. When present, each feature has a predefined likelihood $p(i = 1|C = 1) = p(i = 0|C = 0)$ of exhibiting the concept’s pattern, which can be any detectable change in behavior. If that likelihood is set to zero for a feature, the concept will not influence the feature’s behavior. Similarly, the concept influences the label y after the same change point with likelihood $p(y = 1|C = 1) = p(y = 0|C = 0)$. These parameters are set at the dataset level and samples are drawn according to Algorithm 1.

In this work, we define two concepts, C_1 and C_2 , and two corresponding labels, y_1 and y_2 , influenced by C_1 and C_2 respectively with $p(y|C) = 1$. We generate 10 numerical features with Gaussian background noise, and link C_1 and C_2 to non-overlapping sets of 5 features each. The pattern for all concept-activated features is the emergence of a sinusoid with fixed frequency and amplitude added to the Gaussian noise. The simplicity of this setup ensures that the ground truth is well understood.

We note that our code supports more complex settings, e.g. overlapping concept-feature space or multi-concept label contin-

Algorithm 1: Generating one synthetic time series, given c concepts.

For $C \in C_1, C_2, \dots, C_c$

1. Sample $t_{start} \sim \text{Uniform}(\{1, \dots, T\})$
 2. Sample $C \sim \text{Bernoulli}(0.5)$ to assess “binary behavior” of manifestation.
 3. Sample the label $y_{C_{t_{start}:T}} \sim \text{Bernoulli}(p(y|C))$
 4. For each feature $i \in 1, \dots, d$
 - (a) Sample \mathbf{x}_i ’s behavior as $\lambda_{i,C} \sim \text{Bernoulli}(p(i|C))$
 - (b) Numerical variables are defined by i.i.d. Gaussian noise $\mathbf{x}_i \sim \mathcal{N}(0, 0.5)$. Manifesting concepts are added to the noise after the change point i.e. if $\lambda_{i,C}$ then $\mathbf{x}_{i,t_{start}:T} \sim \mathcal{N}(0, 0.5) + \sin(\mathbf{x}_{i,t_{start}:T})$.
 - (c) Binary variables are defined as $\mathbf{x}_i \sim \text{Bernoulli}(0.5)$. If $\lambda_{i,C}$ then $\mathbf{x}_{i,t_{start}:T} \sim \text{Bernoulli}(0.95)$.
-

gency tables (Appendix A.1). In addition, feature/concept behaviors can be made more realistic (e.g. by including binary variables). Therefore, this dataset is suitable for assessing attributions at both the feature and concept level, and could be used in other scenarios.

Model Training: The model consists of a 3-layer stacked LSTM (Hochreiter and Schmidhuber, 1997) RNN, with 64 hidden units contained in each layer. These layers are followed by a fully connected layer. The model is trained using cross entropy loss with the Adam optimizer (fixed learning rate of $3e-4$) and batch size of 32, over 10000 randomly sampled batches. We report the model performance across all time steps

and examples based on accuracy, AUROC and area under the precision-recall curve (AUPRC).

Concept definition: We use C_1 and C_2 as our concepts. We assign t_{start} as the change point and define the ‘time of interest’ t_{end} as 25 samples (arbitrary choice) after the change point, to ensure the concept is either present (concept group) or absent (control group). We randomly select 100 samples from the validation set to build a CAV for each concept (i.e. C_1 and C_2) and layer l . To ensure that the model is able to identify the concepts, we filter for a minimum model accuracy of 0.8 on a per-sequence basis (arbitrary threshold). The performance of each CAV is assessed on the held-out time steps during the bootstrap procedure, as well as on 500 other time series of the validation set (all time steps).

2.3. Illustration on clinical predictions

Data: We use the de-identified critical care EHR data from the Medical Information Mart for Intensive Care (MIMIC-III) (Johnson et al., 2016a,b; Goldberger et al., 2000) to investigate a real-world application of our technique. After filtering out patients under the age of 18, the MIMIC-III dataset contained 47,296 patients, which were randomised across training (80%), validation (10%), and test (10%) sets. Each patient’s medical history is converted to a time series of one-hour aggregates including different structured data elements (medication, labs, vitals, ...) represented by numerical and binary variables (Tomašev et al., 2019, see Appendix B.1.1 for details).

Model: We focus on the predictions 48 hours in advance of an Acute Kidney Injury (AKI) event of stage 1 or more (max stage 3, as per the Kidney Disease Improving Global Outcomes classification, KDIGO, Khwaja,

2012). We use the same model architecture as described in (Tomašev et al., 2019) which consists in a 3-layer stacked RNN with residual connections and add dropout probability of 0.4 to the output connections of each LSTM cell. The model’s hyper-parameters were defined based on a grid search on the validation set. The model’s performance is then assessed on the test set using AUPRC given the low prevalence of AKI in the dataset. For comparison with the literature, we also report AUROC.

Concept definition: We define illustrative concepts by relying on rule-filtering of specific clinical events from patients included in the validation set. These events then serve to determine t_{start} and t_{end} for the different CAV building strategies. We define two concepts: one that is directly related to the outcome labels for sanity check (referred to as ‘AKI’) and one that is a known risk factor for kidney injury (a specific class of nephrotoxic medication, known to affect renal function). The AKI concept group is defined as follows: admissions where the patient is recorded to have normal renal function (i.e. no AKI, based on the serum creatinine and the KDIGO criteria Khwaja, 2012), and later in the admission renal function degrades to an AKI stage 2 (t_{end}). The control group for the AKI concept is defined as: admissions where no AKI is recorded, with at least one normal creatinine measurement. In this case, a random one-hour bucket is selected as representing the end point of the trajectory, i.e. t_{end} . The AKI concept is purposefully circular to assess how the proposed approach scales to real-world problems.

To define the nephrotoxicity concept, we select admissions where the patient has normal renal function, then receives a particular type of nephrotoxic agent, which is followed by an AKI stage 1, 2 or 3. Please note that we do not select admissions where

the nephrotoxic agent *caused* the AKI, as we do not have that information. We selected one class of nephrotoxic drugs, non-steroidal anti-inflammatory drugs (NSAIDs). The control group for this concept included admissions where the patient had normal renal function followed by an AKI (stage 1, 2 or 3), without receiving an NSAID medication before the adverse event¹.

To avoid potential confounding factors in the CAV, we use the same number of examples in the concept and control groups and choose examples to match on selected data statistics between groups. The features we match on are age, gender, duration of hospital admission, time between admission and AKI (or time between admission and selected t_{end} for controls without AKI events), and inpatient mortality. For each of the patients in the concept and control groups we calculate the vector of features that we wish to match on, standardising based on the training dataset mean and standard deviation. From the pool of candidate examples for the control group, we then select those that minimise the total L1 distance between feature vectors in the control and concept group. The distance minimisation problem is solved using the Munkres algorithm (Munkres, 1957).

We build CAVs for each concept based on selected concept and control groups from the validation set. We then compute tCA and CS on patients from similarly selected groups from the test set.

1. Please note that we control for the endpoint of the trajectory t_{end} to correspond to an AKI event. One could however control for the proportion of AKI samples across both groups. On the other hand, not controlling for the endpoint might introduce a confounding factor where patients receiving NSAIDs have a higher prevalence of AKI.

3. Results

3.1. Synthetic dataset

Data and model: We generate 10,000 time series of 100 time points each to predict y_1 and y_2 . After training, the model reaches 95.34% accuracy, 0.8511 AUPRC and 0.9274 AUROC on a test set of 1,000 time series.

Building the CAV: The different strategies lead to significant CAVs for both C_1 and C_2 as assessed on held-out test sets, although $CAV_{t_{end}-t_{start}}$ has relatively lower performance (see Figure 2a for C_1 and Appendix A.2.1). All CAVs generalize to time points outside of the $[t_{start} : t_{end}]$ time window used for building, on further validation time series. We however note that this result might be driven by the simplicity of our synthetic dataset and the high performance of the RNN model. For compactness, further results focus on the $CAV_{t_{start}:t_{end}}$ strategy. All strategies however lead to similar results in terms of CS and tCA scores.

Presence of the concept over time: tCA is estimated at each time step, using a lag of 25 time steps (arbitrary choice)² for both concepts. Figure 3b displays the average across aligned time series. We observe that tCA has a negative score when the concept is absent, and then sharply transitions to positive scores when the concept becomes present ($t = 50$).

Influence of the CAV: We compute CS at each time point and display global trajectories of the obtained scores in Figure 3c. The results display the expected behavior: for target y_2 , only concept C_2 has CS scores that are not tightly distributed around zero at all time points. In addition, CS scores are low before the change point (here aligned across all time series as $t = 50$), reflecting the

2. We obtain similar results when using a smoothed temporal average instead of a fixed time step.

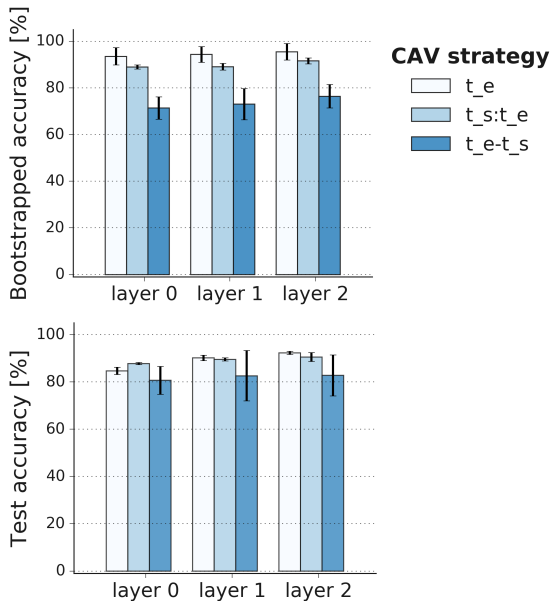


Figure 2: **Synthetic CAV results.** Accuracy of the C_1 CAV in bootstrap (top) and test (bottom) evaluations for $CAV_{t_{end}}$, $CAV_{t_{start}:t_{end}}$ and $CAV_{t_{end}-t_{start}}$, in %.

“absence” of C_1 , while they become positive at the change point, when the label and concept manifest. These results are replicated for target y_1 and C_1 (see Appendix).

3.2. MIMIC dataset

Data and model: Our model predicts AKI of any severity within the next 48 hours with a AUPRC of 0.491 and AUROC of 0.798. It is difficult to make direct comparisons with the literature as, to our knowledge, comparable continuous AKI predictions on MIMIC have not been reported on to date. However, there are a number of similar studies on different EHR datasets: [Simonov et al. \(2019\)](#) report a AUROC of 0.74 for AKI within 24 hours using a discrete time logistic regression triggered after every new measurement; while [Kate et al. \(2020\)](#) report up to 0.724 with a similar setup. [Flechets et al.](#)

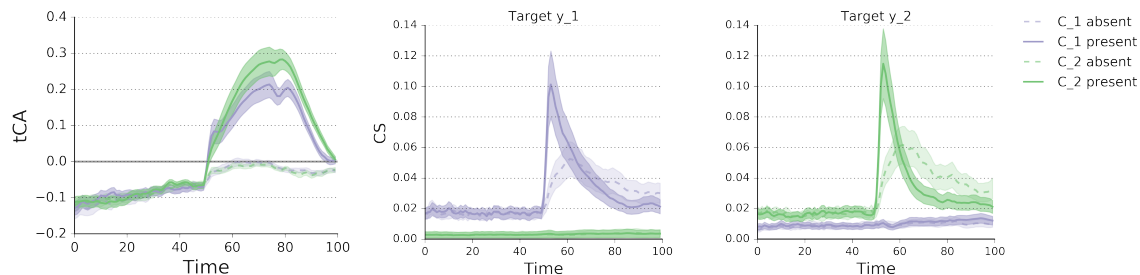


Figure 3: **Concept influence.** (left) tCA scores (layer 2) averaged across time series, and bootstraps (mean \pm std) when a concept (C_1 green, C_2 purple) is absent (light shade, dotted line) or present (dark shade). All timeseries are aligned to have their changepoint at $t = 50$. (right) CS scores for target y_1 (left) and y_2 (right).

(2019) predict AKI within the next 7 days in an ICU population with AUROC ranging from 0.80-0.95 depending on the window of input data.

3.2.1. AKI CONCEPT

Building the CAV: The AKI concept was built using 161 in-patient episodes selected from the validation set. We tested different building strategies, namely $CAV_{t_{end}}$ with t_{end} being the time of AKI, $CAV_{t_{start}:t_{end}}$ using all time steps (subsampling by a factor 2) included in the 12 or 24 hours before AKI and $CAV_{t_{end}-t_{start}}$ by subtracting the activation at time of admission from that of the time of AKI. The obtained linear classifier was then evaluated on examples selected from the test set, on the same points as used for training (i.e. t_{end} , last 12 hours, ...) as well as on all other time points. We observe high training accuracy for all models, as evaluated per the bootstrap scheme (Figure 4a (left), Appendix B.1.4). When evaluating on the test examples, we observe high accuracy on the equivalent time steps as used for training. This accuracy decreases for the concept group when evaluating on test time series (all time steps), with $CAV_{t_{end}}$ and $CAV_{t_{end}-t_{start}}$ seemingly overfitting to the training time steps (Figure 4a

(right)). This result suggests that time steps outside of the selected window might not differentiate the concept and control groups very well, i.e. health states are not that different across AKI and no-AKI patients further away from the adverse event.

Presence of the concept over time: We select the model with best generalization across time steps to compute the alignment, i.e. using the last 24 hours before AKI³ and compute tCA with a lag dt of 24 hours. We present the results using the test examples at time 48 hours before t_{end} (our prediction horizon, t_0 on Figure 4b (left)) and at time t_{end} (corresponding to time of AKI stage 2 for the concept group and a random no AKI event for the control group, t_1).

As previously observed on the synthetic data, using the difference in activations on a 24 hour sliding window leads to higher tCA scores when the concept is present compared to when it is absent, with an increase from t_{start} to t_{end} . We plot the time series of concept alignment for an example patient in Figure 4d for each layer of the model, along with the distribution of tCA scores when using permuted CAV vectors (i.e. built from ran-

3. The obtained results are reproducible with the 12 hours version of $CAV_{t_{start}:t_{end}}$.

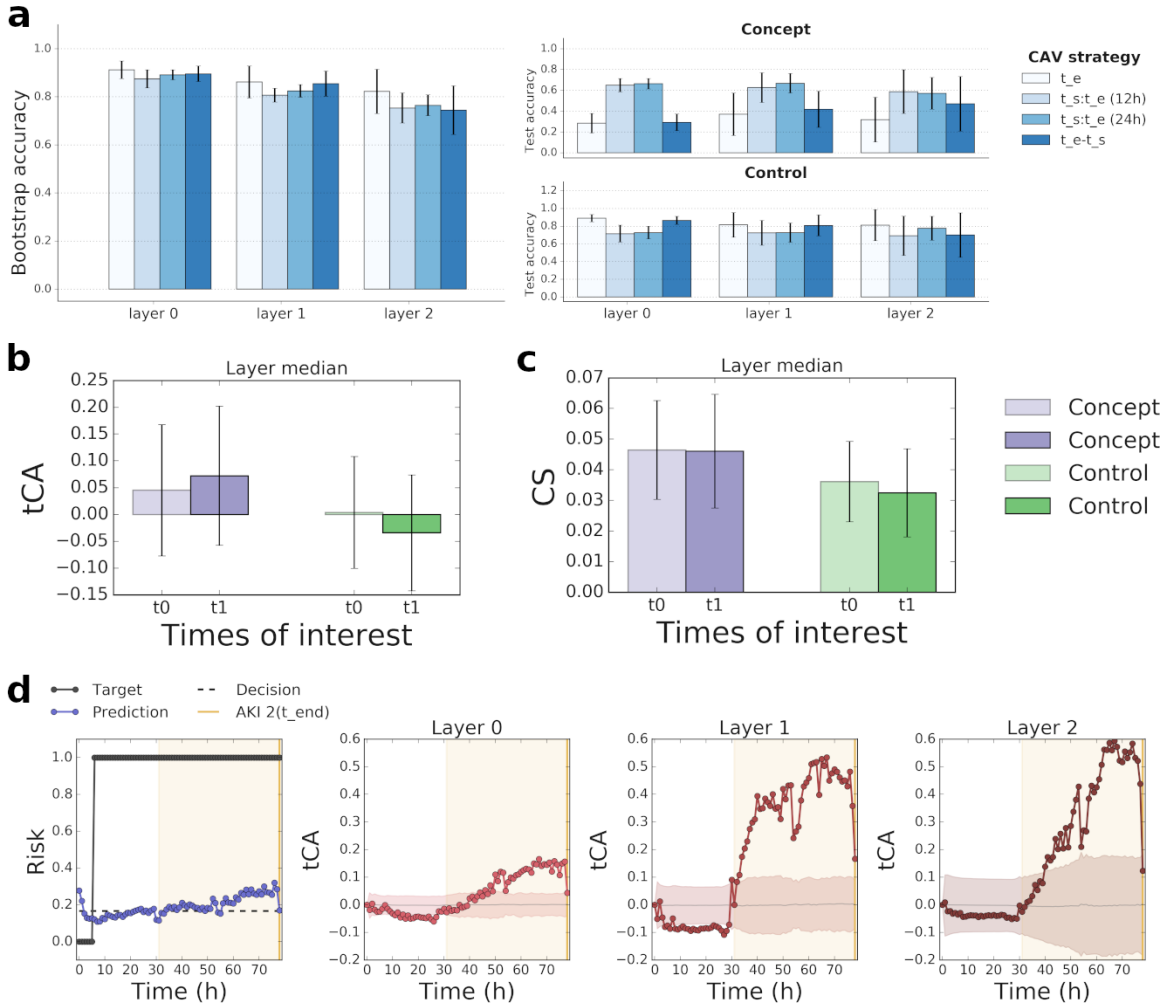


Figure 4: **MIMIC results, AKI concept.** **a** CAV linear model performance on held-out samples (left) and on test samples for concept (top) and control (bottom) samples. Each bar represents a CAV building strategy. **b** tCA global scores, averaged across patients (mean \pm std) for the concept (purple) and control (green) groups 48 hours before AKI (t_0) and at time of AKI stage 2 (t_1). **c** CS scores. **d** Single patient timeseries, displaying the label (AKI 1+ within 48h) and model’s output, as well as tCA for each layer, and its null hypothesis (shaded). The yellow shaded area represents the prediction horizon of the model, i.e. within 48 hours of AKI 2.

domized concept/control labels) for an example from the evaluation group with AKI. The tCA scores per time step seem to reflect the risk as predicted by the model: the tCA score starts increasing around time t 30, i.e.

around 48 hours before the AKI stage 2 event detected by the KDIGO label.

Influence of the CAV: We observe a positive influence of the CAV on the target, as displayed by strictly positive values of CS on

the different samples and time points considered (Figure 4c). This is expected due to the circularity in the definition of this concept.

3.2.2. NSAIDS CONCEPT

Building the CAV: Similarly to the AKI concept, we train three variants of the linear classifier⁴, where we use all samples between 24 hours before AKI to the time of AKI (t_{end}), all samples between the time of NSAIDs and the time of AKI, or the difference in activation between the time of AKI and the time of NSAIDs. While all classifiers are assessed as significant per non-parametric permutation testing, model performance is overall lower than for the AKI concept both for the held-out and validation time steps (Figure 5a, Appendix B.1.5). As previously, we select $CAV_{t_{start}:t_{end}}$ with t_{start} being 24 hours before AKI to evaluate tCA and CS scores.

Presence of the concept over time:

When using a 24-hour sliding window of activation differences, we obtain higher tCA scores at t_{end} when the concept is present compared to at time t_{start} (Figure 5b). This difference is however small and similar scores are obtained for the AKI endpoint on control patients. Figure 5d displays an example trajectory from the evaluation set for $CAV_{t_{start}:t_{end}}$. We discern an increase in alignment, outside of the $\pm 1 \times$ standard deviation, after the time of NSAIDs administration on the three layers. See Appendix B.1.5 for more local examples.

Influence of the CAV: Consistent with our observations, CS displays a small effect of the concept on the predictions at the time of AKI, but the pattern is not as clear as for the AKI concept (Figure 5c). This could reflect either that the CAV does not prop-

erly represent the NSAIDs direction, or that the model is not significantly influenced by this direction when making predictions. Further work will investigate other nephrotoxic agents as well as involve a clinical evaluation of patients to ensure that the agent *caused* the AKI.

4. Discussion and future work

In this work, we explore the use of TCAV for RNNs, by defining concepts as trajectories over time. Across datasets and concepts, we notice that $CAV_{t_{start}:t_{end}}$ consistently leads to better generalization across time points. This result suggests that a majority of time steps in the time windows selected were relevant for the considered concepts. However, extending this window or increasing the variability of the signals within this window might lead to different results. Nevertheless, we show that this approach provides meaningful CAVs and that both tCA and CS scores are consistent with our expectations on the synthetic data. We observe that tCA , as a temporal “derivative”, saturates if the concept’s presence or absence does not vary over the time window $[t - dt, t]$. Similarly, CS highlights transitions in the model’s predictions when taking the gradients w.r.t. the sigmoid of the logits, as the sigmoid saturates when the prediction is further away from the decision boundary. This could suggest a better use case of tCA and CS in alert-based settings, where predictions/explanations are provided at specific time points, e.g. when the predicted risk passes the decision threshold.

While our approach factors in temporality in the construction of CAVs and tCA , CS would need to be extended to be able to account for how differences in model predictions relate to changes in the presence/absence of a concept *over time*. In this regard, a potential direction of work would

4. Given that the end point (AKI 1+) is controlled for, $CAV_{t_{end}}$ is not built.

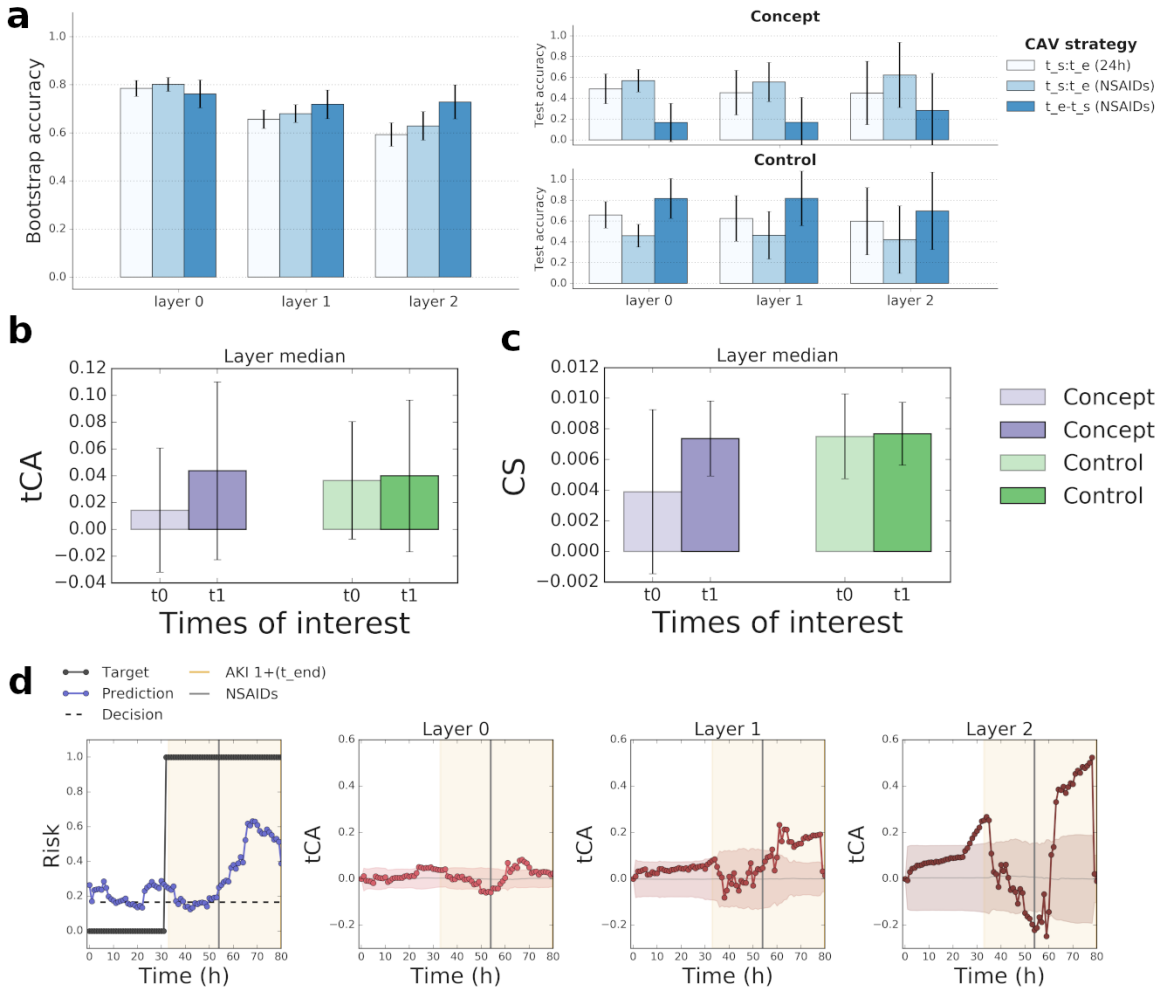


Figure 5: **MIMIC results, NSAIDs concept.** **a** CAV linear model performance on held-out samples (left) and on test samples for concept (top) and control (bottom) samples. Each bar represents a CAV building strategy. **b** tCA global scores, averaged across patients (mean \pm std) for the concept (purple) and control (green) groups 48 hours before AKI (t_0) and at time of AKI stage 2 (t_1). **c** CS scores. **d** Single patient timeseries, displaying the label (AKI 1+ within 48h) and model’s output, as well as tCA for each layer, and its null hypothesis (shaded). The yellow shaded area represents the prediction horizon of the model, i.e. within 48 hours of AKI 1+. The administration of NSAIDs is displayed by a grey vertical line.

be to refer to Temporal Integrated Gradients (Hardt et al., 2019). Such a method based on integrated gradients (Sundararajan et al., 2017) would also enable the use of the proposed approach for local explanations, as in-

tegrated gradients estimate the difference between the obtained prediction and a “neutral decision”.

One limitation of TCAV arises from the difficulty of defining a concept through ex-

amples from real-world EHR data. While toy datasets or ImageNet applications seem intuitive, healthcare data can be difficult to separate into clinical concepts. In the present work, we computed relative CAVs by selecting concept and control examples and matched control examples for a number of criteria. We note that other matching criteria and methods could be used, e.g. propensity score matching or other optimal transport techniques. While we reported promising results using these CAVs, a danger is to miss confounding factors that then lead to a significant CAV. A future direction could be to generate counterfactuals, as in (Goyal et al., 2019; Pfohl et al., 2019; Singla et al., 2019). Given the dimensionality of the data, training and evaluating such a counterfactual generative model however remains challenging. Another risk lies in potential confirmation bias during the process of building the CAV and estimating tCA and CS scores, as the user might be tuning the CAV building until a concept surfaces. It could hence be desirable to know how much signal is covered by a set of concepts, as proposed in (Yeh et al., 2019). On the other hand, the clinical user might want to define a limited set of “actionable” concepts, e.g. “dehydration” or “nephrotoxicity”, for which a clinical action could prevent the predicted outcome. This would alleviate the concerns around building the “complete” set of concepts, and provide a path to action, especially in the case of local explanations.

Finally, we evaluate the proposed approach empirically, based on the ‘ground truth’ present in the synthetic data. The clinical relevance and utility of TCAV for EHR should be more rigorously assessed using human and task grounded evaluations, as suggested in (Doshi-Velez and Kim, 2018). In particular, it would be useful to investigate whether concept-based explanations can help guide clinical actions taken in response

to a prediction, and, ultimately, whether these explanations improve outcomes for patients.

Software and Data

The Python and TensorFlow code to generate the synthetic dataset, models, and compute CS and tCA is available at <https://github.com/google/ehr-predictions/tree/master/tcav-for-ehr>. The de-identified EHR data is available based on a user agreement at <https://physionet.org/content/mimiciii/1.4/>.

Acknowledgments

We thank Been Kim and Yash Goyal for discussions and for sharing code.

References

- R. Ambrosino, B G Buchanan, G F Cooper, and M J Fine. The use of misclassification costs to learn rule-based decision support models for cost-effective hospital admission strategies. *Proceedings. Symposium on Computer Applications in Medical Care*, pages 304–8, 1995. ISSN 0195-4210. URL <http://www.ncbi.nlm.nih.gov/pubmed/8563290><http://www.pubmedcentral.nih.gov/articlerender.fcgi?artid=PMC2579104>.
- Rich Caruana, Yin Lou, Johannes Gehrke, Paul Koch, Marc Sturm, and Noemie Elhadad. Intelligible Models for HealthCare. In *Proceedings of the 21th ACM SIGKDD International Conference on Knowledge Discovery and Data Mining - KDD '15*, pages 1721–1730, 2015. ISBN 9781450336642. doi: 10.1145/2783258.2788613. URL <http://dx.doi.org/10.1145/2783258>.

- 2788613<http://dl.acm.org/citation.cfm?doid=2783258.2788613>.
- Edward Choi, Mohammad Taha Bahadori, Joshua A. Kulas, Andy Schuetz, Walter F. Stewart, and Jimeng Sun. RE-TAIN: An interpretable predictive model for healthcare using reverse time attention mechanism. In *Advances in Neural Information Processing Systems*, pages 3512–3520. Neural information processing systems foundation, 2016.
- Finale Doshi-Velez and Been Kim. Considerations for Evaluation and Generalization in Interpretable Machine Learning. pages 3–17. Springer edition, 2018. doi: 10.1007/978-3-319-98131-4_1.
- Marine Flechet, Stefano Falini, Claudia Bonetti, Fabian Güiza, Miet Schetz, Greet Van den Berghe, and Geert Meyfroidt. Machine learning versus physicians’ prediction of acute kidney injury in critically ill adults: a prospective evaluation of the akipredictor. *Critical Care*, 23(1):282, Aug 2019. ISSN 1364-8535. doi: 10.1186/s13054-019-2563-x. URL <https://doi.org/10.1186/s13054-019-2563-x>.
- Joseph Futoma, Sanjay Hariharan, Katherine Heller, Mark Sendak, Nathan Brajer, Meredith Clement, Armando Bedoya, and Cara O’Brien. An Improved Multi-Output Gaussian Process RNN with Real-Time Validation for Early Sepsis Detection. Technical report, 2017.
- A. L. Goldberger, L. A. Amaral, L. Glass, J. M. Hausdorff, P. C. Ivanov, R. G. Mark, J. E. Mietus, G. B. Moody, C. K. Peng, and H. E. Stanley. PhysioBank, PhysioToolkit, and PhysioNet: components of a new research resource for complex physiologic signals. *Circulation*, 101(23), 2000. ISSN 15244539. doi: 10.1161/01.cir.101.23.e215.
- Yash Goyal, Uri Shalit, and Been Kim. Explaining Classifiers with Causal Concept Effect (CaCE). jul 2019. URL <http://arxiv.org/abs/1907.07165>.
- Michaela Hardt, Alvin Rajkomar, Gerardo Flores, Andrew Dai, Michael Howell, Greg Corrado, Claire Cui, and Moritz Hardt. Explaining an increase in predicted risk for clinical alerts. Technical report, 2019. URL <https://arxiv.org/abs/1907.04911>.
- Sepp Hochreiter and Juergen Schmidhuber. Long Short-Term Memory. *Neural Computation*, 9(8):1735–1780, 1997. URL <http://www7.informatik.tu-muenchen.de/~hochreith><http://www.idsia.ch/~juergen>.
- Alistair E.W. Johnson, Tom J Pollard, and Roger G. Mark. MIMIC-III Clinical Database., 2016a.
- Alistair E.W. Johnson, Tom J. Pollard, Lu Shen, Li Wei H. Lehman, Mengling Feng, Mohammad Ghassemi, Benjamin Moody, Peter Szolovits, Leo Anthony Celi, and Roger G. Mark. MIMIC-III, a freely accessible critical care database. *Scientific Data*, 3, may 2016b. ISSN 20524463. doi: 10.1038/sdata.2016.35.
- Rohit J. Kate, Noah Pearce, Debesh Mazumdar, and Vani Nilakantan. A continual prediction model for inpatient acute kidney injury. *Computers in Biology and Medicine*, 116:103580, 2020. ISSN 0010-4825. doi: <https://doi.org/10.1016/j.compbiomed.2019.103580>. URL <http://www.sciencedirect.com/science/article/pii/S0010482519304342>.
- Arif Khwaja. KDIGO clinical practice guidelines for acute kidney injury, oct 2012. ISSN 16602110.

- Been Kim, Martin Wattenberg, Justin Gilmer, Carrie Cai, James Wexler, Fernanda Viegas, and Rory Sayres. Interpretability beyond feature attribution: Quantitative Testing with Concept Activation Vectors (TCAV). In *35th International Conference on Machine Learning, ICML 2018*, volume 6, pages 4186–4195, 2018. ISBN 9781510867963. URL <http://arxiv.org/abs/1711.11279>.
- Jean-Philippe Lafrance and Donald R. Miller. Selective and non-selective non-steroidal anti-inflammatory drugs and the risk of acute kidney injury. *Pharmacoepidemiology and Drug Safety*, 18(10):923–931.
- Zachary C. Lipton, David C. Kale, Charles Elkan, and Randall Wetzel. Learning to diagnose with LSTM recurrent neural networks. In *4th International Conference on Learning Representations, ICLR 2016 - Conference Track Proceedings*. International Conference on Learning Representations, ICLR, nov 2016.
- James Munkres. Algorithms for the Assignment and Transportation Problems. *Journal of the Society for Industrial and Applied Mathematics*, 5(1):32–38, mar 1957. ISSN 0368-4245. doi: 10.1137/0105003.
- Cecilia Panigutti, Alan Perotti, Dino Pedreschi, and Dino 2020 Pedreschi. An ontology-based approach to black-box sequential data classification explanations. 2020. doi: 10.1145/3351095.3372855. URL <https://doi.org/10.1145/3351095.3372855>.
- Seyedeh Neelufar Payrovnaziri, Zhaoyi Chen, Pablo Rengifo-Moreno, Tim Miller, Jiang Bian, Jonathan H Chen, Xiuwen Liu, and Zhe He. Explainable artificial intelligence models using real-world electronic health record data: a systematic scoping review. *Journal of the American Medical Informatics Association*, 2020. ISSN 1527-974X. doi: 10.1093/jamia/ocaa053. URL <https://doi.org/10.1093/jamia/ocaa053>.
- Stephen Pfohl, Tony Duan, Daisy Yi Ding, and Nigam H Shah. Counterfactual Reasoning for Fair Clinical Risk Prediction. In *Proceedings of Machine Learning Research*, volume 85, pages 1–29, 2019.
- Laura Plantinga, Vanessa Grubbs, Urmimala Sarkar, Chi-Yuan Hsu, Elizabeth Hedgeman, Bruce Robinson, Rajiv Saran, Linda Geiss, Nilka Ríos Burrows, Mark Eberhardt, Neil Powe, and CDC CKD Surveillance Team. Nonsteroidal anti-inflammatory drug use among persons with chronic kidney disease in the united states. *Annals of family medicine*, 9(5): 423–430, 2011.
- Alvin Rajkomar, Eyal Oren, Kai Chen, Andrew M. Dai, Nissan Hajaj, Michaela Hardt, Peter J. Liu, Xiaobing Liu, Jake Marcus, Mimi Sun, Patrik Sundberg, Hector Yee, Kun Zhang, Yi Zhang, Gerardo Flores, Gavin E. Duggan, Jamie Irvine, Quoc Le, Kurt Litsch, Alexander Mossin, Justin Tansuwan, De Wang, James Wexler, Jimbo Wilson, Dana Ludwig, Samuel L. Volchenbom, Katherine Chou, Michael Pearson, Srinivasan Madabushi, Nigam H. Shah, Atul J. Butte, Michael D. Howell, Claire Cui, Greg S. Corrado, and Jeffrey Dean. Scalable and accurate deep learning with electronic health records. *npj Digital Medicine*, 1(1), dec 2018. ISSN 2398-6352. doi: 10.1038/s41746-018-0029-1.
- Ying Sha and May D. Wang. Interpretable predictions of clinical outcomes with an attention-based recurrent neural network. In *ACM-BCB 2017 - Proceedings*

- of the 8th ACM International Conference on Bioinformatics, Computational Biology, and Health Informatics, pages 233–240, New York, NY, USA, aug 2017. Association for Computing Machinery, Inc. ISBN 9781450347228. doi: 10.1145/3107411.3107445. URL <https://dl.acm.org/doi/10.1145/3107411.3107445>.
- Benjamin Shickel, Tyler J. Loftus, Lasith Adhikari, Tezcan Ozrazgat-Baslanti, Azra Bihorac, and Parisa Rashidi. DeepSOFA: A Continuous Acuity Score for Critically Ill Patients using Clinically Interpretable Deep Learning. *Scientific Reports*, 9(1), dec 2019. ISSN 20452322. doi: 10.1038/s41598-019-38491-0.
- Michael Simonov, Ugochukwu Ugwuowo, Erica Moreira, Yu Yamamoto, Aditya Biswas, Melissa Martin, Jeffrey Testani, and F. Perry Wilson. A simple real-time model for predicting acute kidney injury in hospitalized patients in the us: A descriptive modeling study. *PLOS Medicine*, 16(7):1–15, 07 2019. doi: 10.1371/journal.pmed.1002861. URL <https://doi.org/10.1371/journal.pmed.1002861>.
- Sumedha Singla, Brian Pollack, Junxiang Chen, and Kayhan Batmanghelich. Explanation by Progressive Exaggeration. 2019. URL <http://arxiv.org/abs/1911.00483>.
- Mukund Sundararajan, Ankur Taly, and Qiqi Yan. Axiomatic attribution for deep networks. In *34th International Conference on Machine Learning, ICML 2017*, volume 7, pages 5109–5118, 2017. ISBN 9781510855144.
- Nenad Tomašev, Xavier Glorot, Jack W. Rae, Michal Zielinski, Harry Askham, Andre Saraiva, Anne Mottram, Clemens Meyer, Suman Ravuri, Ivan Protsyuk, Alistair Connell, Cían O. Hughes, Alan Karthikesalingam, Julien Cornebise, Hugh Montgomery, Geraint Rees, Chris Laing, Clifton R. Baker, Kelly Peterson, Ruth Reeves, Demis Hassabis, Dominic King, Mustafa Suleyman, Trevor Back, Christopher Nielson, Joseph R. Ledsam, and Shakir Mohamed. A clinically applicable approach to continuous prediction of future acute kidney injury. *Nature*, 572(7767):116–119, aug 2019. ISSN 0028-0836. doi: 10.1038/s41586-019-1390-1.
- Sana Tonekaboni, Shalmali Joshi, Melissa D McCradden, and Anna Goldenberg. What Clinicians Want: Contextualizing Explainable Machine Learning for Clinical End Use. In *Proceedings of Machine Learning Research*, pages 1 – 21, 2019. URL <http://arxiv.org/abs/1905.05134>.
- Cao Xiao, Edward Choi, and Jimeng Sun. Opportunities and challenges in developing deep learning models using electronic health records data: A systematic review. *Journal of the American Medical Informatics Association*, 25(10):1419–1428, 2018. ISSN 1527974X. doi: 10.1093/jamia/ocy068. URL <https://academic.oup.com/jamia/article-abstract/25/10/1419/5035024>.
- Chih-Kuan Yeh, Been Kim, Sercan O. Arik, Chun-Liang Li, Pradeep Ravikumar, and Tomas Pfister. On Concept-Based Explanations in Deep Neural Networks. In *Proceedings of the 33rd Conference on Neural Information Processing Systems (NeurIPS 2019)*, 2019. URL <http://arxiv.org/abs/1910.07969>.

Appendix A. Synthetic data

A.1. Data generation

The dataset has been designed to allow for multiple different scenarios (Figure 6). For simplicity, the data generation process used throughout the main text relies on scenario **a** of Figure 6.

A.2. Concept-based explanations

A.2.1. CAV BUILDING

We display the balanced accuracy and ROC AUC of the linear CAV classifiers evaluated on held-out samples, as well as on further time series (including time points outside the $[t_{start} : t_{end}]$ window) for each building strategy in tables Table 1 (CAV $_{t_{start}:t_{end}}$), Table 2 (CAV $_{t_{end}}$) and Table 3 (CAV $_{t_{end}-t_{start}}$).

Figure 7 illustrates the balanced accuracy (in %) for the linear classifier defining C_2 .

A.2.2. INFLUENCE OF THE CAV

We display the global CS scores for each layer and target when the concepts are present or absent in Figure 8.

Figure 9 displays global CS scores per time point across the different categories of positive and negative predictions that the model makes.

Appendix B. Application to MIMIC

B.1. Data and modeling

B.1.1. DATA REPRESENTATION

The de-identified EHR data were mapped to the Fast Healthcare Interoperability Resource (FHIR) specification as described in Rajkomar et al. (2018). From these records, we extracted the following feature categories: admission metadata, observations, procedures, diagnoses, laboratory tests, medication orders and vital signs. No free-text clinical notes were used. These records were organised into a sequential patient representation, where all data for a single patient were ordered by time, subdivided into admissions and then bucketed into 1-hour time steps, taking the median of any features present multiple times per time step. Continuous features were associated with an additional binary presence variable to indicate whether the feature was present or absent at that time step. No feature imputation was applied. Categorical features were one-hot encoded. All features were trimmed at the 1 and 99 percentiles, and standardized.

B.1.2. MODEL ARCHITECTURE AND TRAINING

We use the model architecture described in Tomašev et al. (2019) to predict acute kidney injury in a range of future prediction windows ranging from 6h ahead to 72h. In particular, the model used in this analysis comprises 2 embedding layers of size 400 with residual connections and an RNN architecture using a GRU cell of 200 units per layer and 3 layers. We use a batch size of 128, a back propagation through time window of 128, and an initial learning rate of 0.001 that decays every 12,000 steps by a factor of 0.85. These parameters were selected via a grid search using the validation set. Learning is

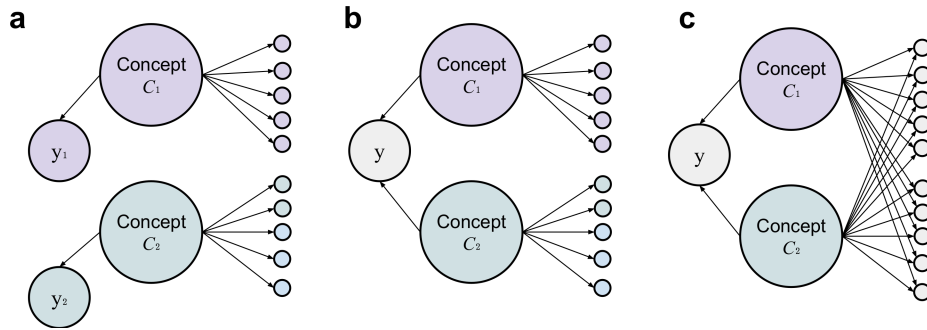


Figure 6: Illustration of the causal graph and potential uses. **a** Concepts sampled independently, each affecting non-overlapping sets of features and different labels. **b** The concepts jointly affect the label (e.g. using AND or OR). **c** The concepts jointly affect the label and all features.

Table 1: Performance of CAVs on held-out and test samples, $CAV_{t_{start}:t_{end}}$ building strategy.

| Concept | Layer | Accuracy [%] | ROC AUC [%] | Accuracy on test [%] |
|---------|-------|--------------|-------------|----------------------|
| C_1 | 0 | 88.97 | 95.89 | 87.72 |
| C_1 | 1 | 89.08 | 96.12 | 89.44 |
| C_1 | 2 | 91.55 | 97.33 | 90.52 |
| C_2 | 0 | 91.78 | 97.12 | 86.67 |
| C_2 | 1 | 91.18 | 97.11 | 89.15 |
| C_2 | 2 | 92.93 | 97.51 | 90.65 |

Table 2: Performance of CAVs on held-out and test samples, $CAV_{t_{end}}$ building strategy.

| Concept | Layer | Accuracy [%] | ROC AUC [%] | Accuracy on test [%] |
|---------|-------|--------------|-------------|----------------------|
| C_1 | 0 | 93.51 | 98.27 | 85.08 |
| C_1 | 1 | 94.34 | 99.55 | 90.31 |
| C_1 | 2 | 95.46 | 99.53 | 92.51 |
| C_2 | 0 | 85.29 | 93.41 | 83.40 |
| C_2 | 1 | 89.90 | 96.24 | 91.02 |
| C_2 | 2 | 92.15 | 97.11 | 91.22 |

stopped after the earlier of 100,000 steps or AUPRC convergence on the task of predicting AKI 48 hours ahead of time. The model is evaluated on the test set using AUPRC: we observe AUPRC of 41.0% for the task of predicting any severity of AKI in the next 24 hours, and AUPRC of 44.6% for the task of predicting any severity of AKI in the next 48 hours.

Table 3: Performance of CAVs on held-out and test samples, $CAV_{t_{end}-t_{start}}$ building strategy. Non-significant results after correction for multiple comparisons are emphasized.

| Concept | Layer | Accuracy [%] | ROC AUC [%] | Accuracy on test [%] |
|---------|-------|--------------|-------------|----------------------|
| C_1 | 0 | 71.37 | 80.25 | 81.10 |
| C_1 | 1 | 73.04* | 83.37* | 82.96 |
| C_1 | 2 | 76.40 | 86.54 | 83.15 |
| C_2 | 0 | 69.96 | 79.14 | 76.35 |
| C_2 | 1 | 72.31* | 79.29* | 84.35 |
| C_2 | 2 | 74.21* | 83.18* | 82.37 |

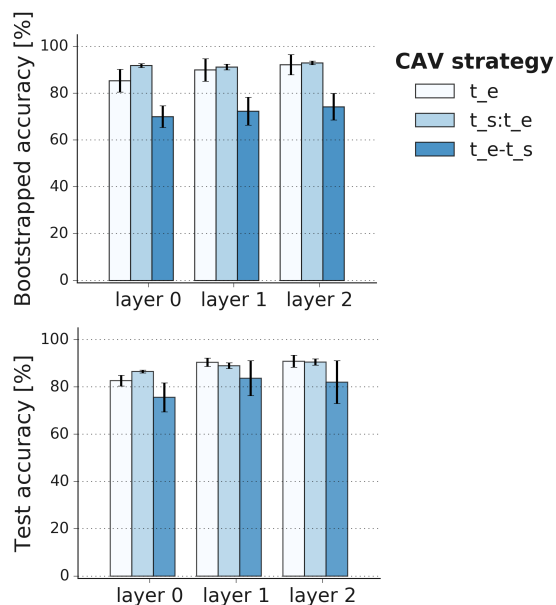


Figure 7: **Synthetic CAV results.** Accuracy of the C_2 CAV in bootstrap (top) and test (bottom) evaluations for $CAV_{t_{end}}$, $CAV_{t_{start}:t_{end}}$ and $CAV_{t_{end}-t_{start}}$, in %.

B.1.3. NSAIDS DEFINITION

Our computable definition for NSAID exposure was based on the US Food and Drug Administration (FDA) Established Pharmacological Class (EPC) grouping, with two ad-

ditional COX-2 selective NSAIDs that were used historically but are no longer on this list (rofecoxib and valdecoxib). The complete list of drugs included is presented in table 4. Previous studies on NSAID-mediated nephrotoxicity have either excluded aspirin and acetaminophen due to their widespread use at low doses (Plantinga et al., 2011) or only used high-dose aspirin (Lafrance and Miller); however aspirin is excluded here to avoid the need for dose calculations in this preliminary work.

Table 4: List of NSAID medications included in the *nephrotoxicity* concept.

| MEDICATION NAME | |
|-----------------|----------------|
| BROMFENAC | KETOROLAC |
| CELECOXIB | MEFENAMIC ACID |
| DICLOFENAC | MELOXICAM |
| DIFLUNISAL | NABUMETONE |
| ETODOLAC | NAPROXEN |
| FENOPROFEN | OXAPROZIN |
| FLURBIPROFEN | PIROXICAM |
| IBUPROFEN | ROFECOXIB |
| INDOMETHACIN | SULINDAC |
| KETOPROFEN | VALDECOXIB |

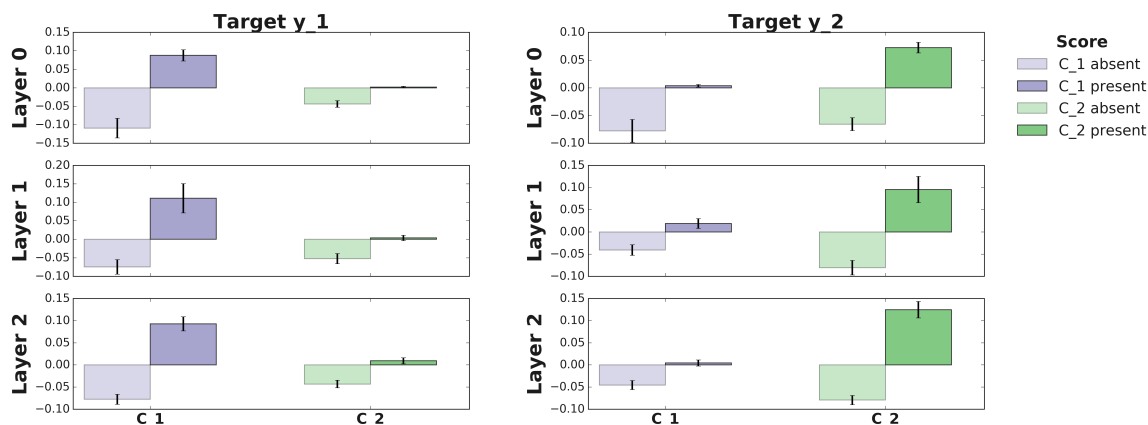


Figure 8: CS scores as averaged across all time steps and bootstraps (mean \pm std) for each target and layer when a concept (C_1 purple, C_2 green) is absent (light shade) or present (dark shade).

B.1.4. CONCEPT EXPLANATIONS OF AKI

CAV building Table 5 displays the performance of the CAV linear classifier as evaluated on held-out samples from the bootstrap scheme. All building strategies lead to significant linear classifiers. When evaluated on time series from different patients, we however notice that performance decreases significantly for $CAV_{t_{end}}$ (accuracy $\sim 30\%$ for concept group time steps) and $CAV_{t_{end}-t_{start}}$ (accuracy $\sim 40\%$ for concept group time steps). This result suggests that those strategies, which focus most on t_{end} might be overfitting to this specific time step.

other time series and time steps (consistent accuracy for both control and concept time series, $\sim 55 - 65\%$, compared to unstable results for $CAV_{t_{end}-t_{start}}$).

Local examples The next figures display local examples for the NSAIDs concept (true positives: Figure 10, negative predictions: Figure 11, fals positive prediction: Figure 12).

B.1.5. CONCEPT EXPLANATIONS FOR NSAIDs

CAV building Table 6 displays the performance of the CAV linear classifier as evaluated on held-out samples from the bootstrap scheme. The results suggest that the difference between the concept and control groups is more subtle, which is not unexpected. As for the AKI concept, the $CAV_{t_{start}:t_{end}}$ seems to generalize better to

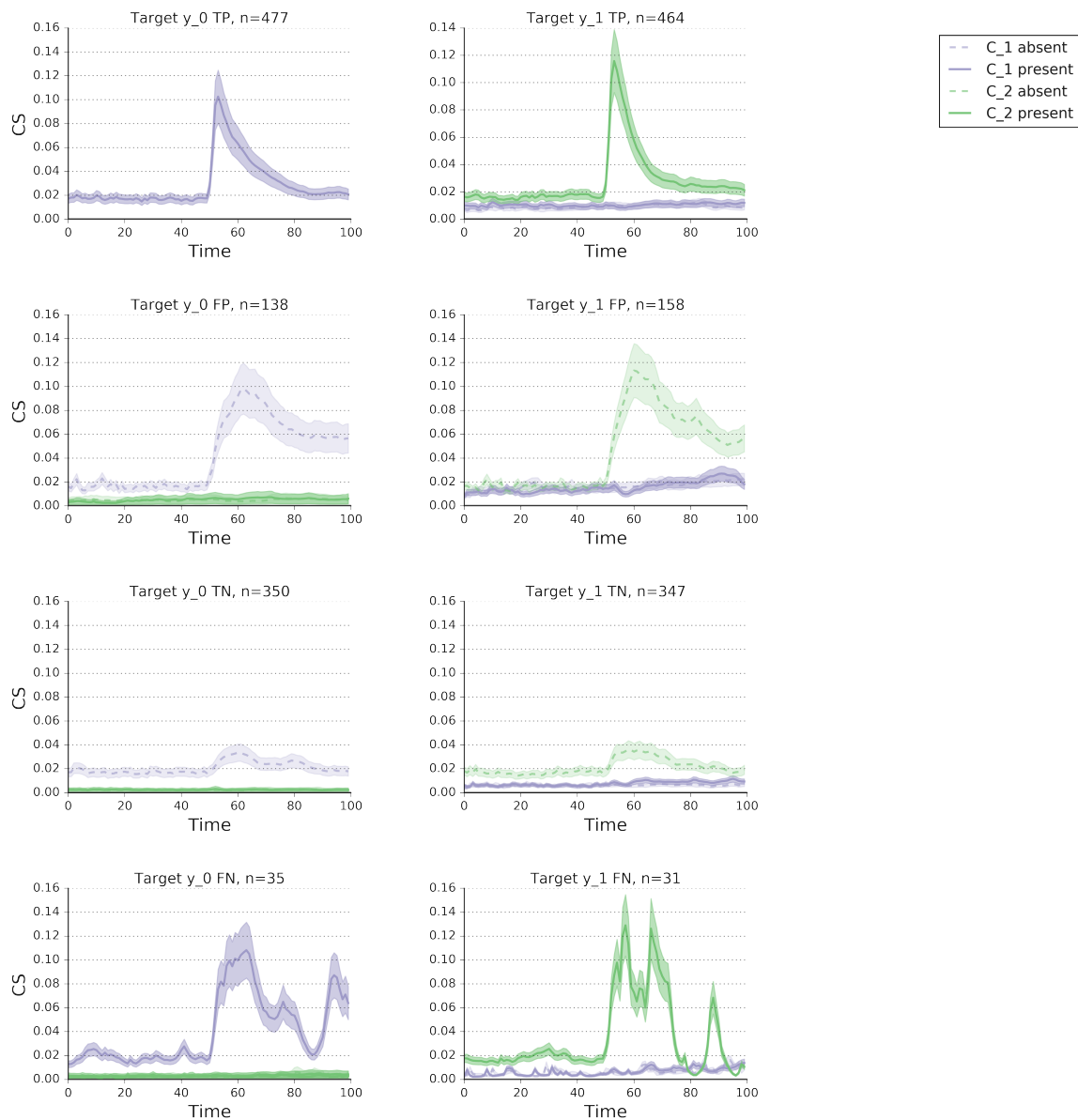


Figure 9: CS scores at layer 2 as averaged across all time series (mean \pm std) for each target when a concept (C_1 green, C_2 purple) is absent (light shade, dotted) or present (dark shade), for correct (TP, TN) and incorrect (FP, FN) predictions. n represents the number of trajectories considered for averaging.

Table 5: Performance of CAV classifier for the *AKI* concept on MIMIC, averaged across 100 bootstrap resamples.

| CAV building strategy | Layer | $n_{concept}$ | $n_{control}$ | Accuracy [%] | ROC AUC [%] |
|---|-------|---------------|---------------|--------------|-------------|
| Last 12h ($CAV_{t_{start}:t_{end}}$) | 0 | | | 87.03 | 94.60 |
| | 1 | 317 | 306 | 80.18 | 90.03 |
| | 2 | | | 75.64 | 87.92 |
| Last 24h ($CAV_{t_{start}:t_{end}}$) | 0 | | | 88.53 | 95.03 |
| | 1 | 599 | 572 | 82.04 | 89.67 |
| | 2 | | | 76.15 | 86.96 |
| Time of AKI ($CAV_{t_{end}}$) | 0 | | | 91.17 | 96.62 |
| | 1 | 81 | 80 | 86.95 | 96.12 |
| | 2 | | | 80.81 | 92.29 |
| AKI - 12h ($CAV_{t_{end}-t_{start}}$) | 0 | | | 90.00 | 95.72 |
| | 1 | 81 | 80 | 85.22 | 95.03 |
| | 2 | | | 74.97 | 89.01 |

Table 6: Performance of CAV classifier for the *NSAIDs* concept on MIMIC, averaged across 100 bootstrap resamples.

| CAV building strategy | Layer | $n_{concept}$ | $n_{control}$ | Accuracy [%] | ROC AUC [%] |
|---|-------|---------------|---------------|--------------|-------------|
| Last 24h ($CAV_{t_{start}:t_{end}}$) | 0 | | | 79.63 | 88.02 |
| | 1 | 480 | 472 | 66.47 | 75.62 |
| | 2 | | | 60.34 | 70.59 |
| NSAIDs to AKI ($CAV_{t_{start}:t_{end}}$) | 0 | | | 82.93 | 91.28 |
| | 1 | 503 | 470 | 70.70 | 81.49 |
| | 2 | | | 65.70 | 78.27 |
| AKI - NSAIDs ($CAV_{t_{end}-t_{start}}$) | 0 | | | 75.15 | 83.71 |
| | 1 | 65 | 65 | 72.15 | 82.55 |
| | 2 | | | 67.92 | 84.43 |

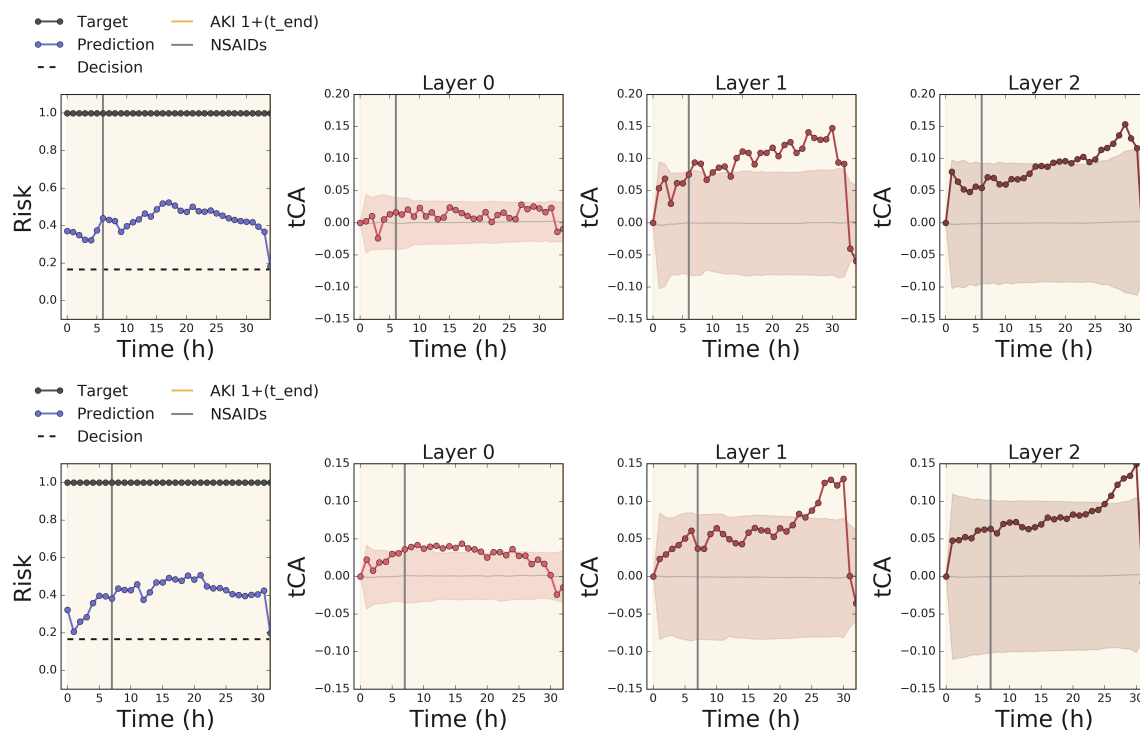


Figure 10: **Local MIMIC results, NSAIDs concept, true positives.** Single patient timeseries, displaying the label (AKI 1+ within 48h) and model's output, as well as tCA for each layer, and its null hypothesis (shaded). The yellow shaded area represents the prediction horizon of the model, i.e. 48 hours. The administration of NSAIDs is displayed by a grey vertical line. The first 2 rows display increases in tCA in true positive predictions, the middle 2 rows display no or negative alignment for negative predictions and the last row displays an increase in alignment at time of NSAIDs administration in a false positive prediction.

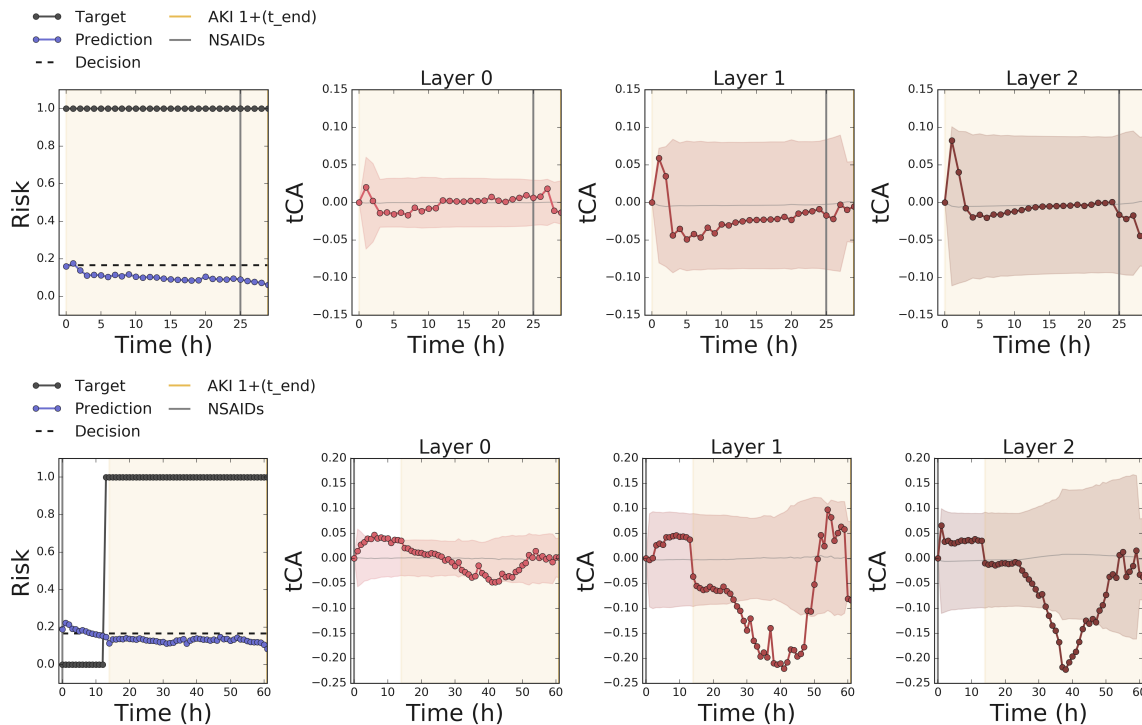


Figure 11: **Local MIMIC results, NSAIDs concept, negative predictions.** The plots display no or negative alignment for negative predictions.

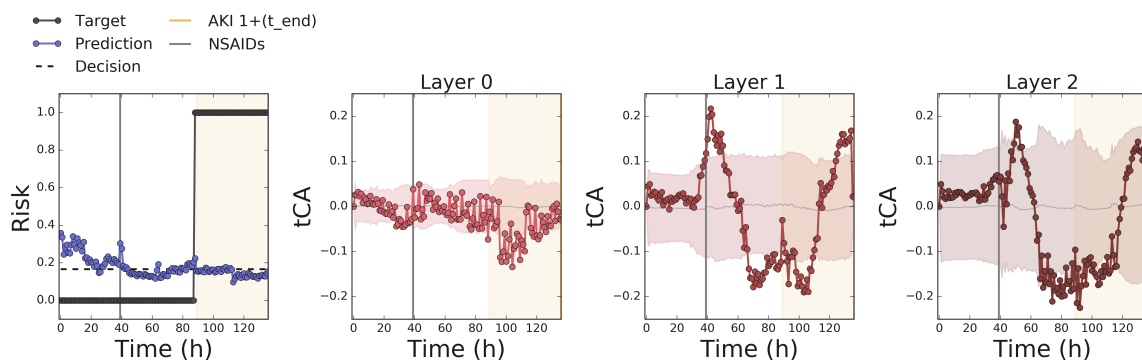


Figure 12: **Local MIMIC results, NSAIDs concept, false positive.** The plots display an increase in alignment at time of NSAIDs administration in a false positive prediction (around $t = 40$).